Nanoscale

Accepted Manuscript

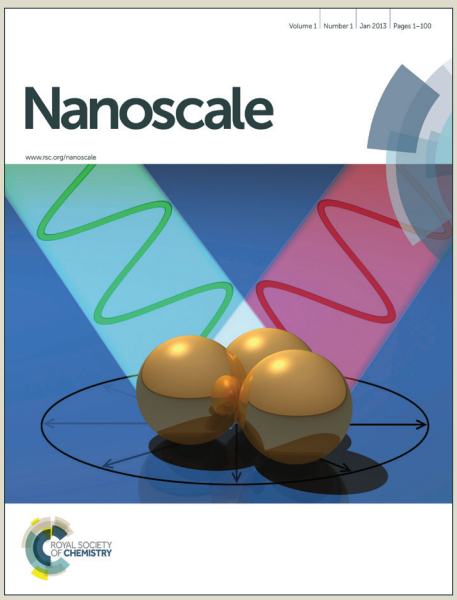

ROYAL SOCIETY OF CHEMISTRY

www.rsc.org/nanoscale

Journal Name

RSCPublishing

ARTICLE

Urchin like $Ni_xCo_{3-x}O_4$ hierarchical nanostructures as non-precious, bifunctional electrocatalyst for anion exchange membrane alkaline alcohol fuel cells†

Cite this: DOI: 10.1039/x0xx00000x

Received ooth xxx 2014,
Accepted ooth xxx 2014

DOI: 10.1039/x0xx00000x

www.rsc.org/

Palanisamy Manivasakan, Parthiban Ramasamy and Jinkwon Kim*

This work contributes to the development of non-precious, bifunctional electrocatalyst for dioxygen reduction and methanol oxidation reaction that is considered as a candidate of the cathode and anode materials for anion exchange membrane (AEM) alkaline alcohol fuel cells in future. A series of nickel doped cobalt oxide ($Ni_xCo_{3-x}O_4$) hierarchical nanostructures composed with 1D nanorods were prepared by an inexpensive hydrothermal method. X-ray diffraction patterns make visible that the $Ni_xCo_{3-x}O_4$ crystallize in a cubic spinel phase. The electrochemical performances of catalysts were investigated by conventional cyclic voltammetric (CV) technique. Comparative electrocatalytic behaviour of $Ni_xCo_{3-x}O_4$ hierarchical nanostructures were explored with Co_3O_4 and $Co_{0.33}Ni_{0.67}O$. The synergistic behaviors of nickel in $Ni_xCo_{3-x}O_4$ were established with respect to nickel content. $Ni_xCo_{3-x}O_4$ hierarchical nanostructures exhibits better catalytic behaviour than Co_3O_4 and $Co_{0.33}Ni_{0.67}O$. Even though all the compositions of $Ni_xCo_{3-x}O_4$ show better catalytic behaviour, $Ni_1Co_2O_4$ is identified as a superior bi-functional electrocatalyst for oxygen reduction and methanol oxidation reaction in alkaline media. Function of nickel content on the electrocatalytic properties of $Ni_xCo_{3-x}O_4$ hierarchical nanostructures are clearly revealed in this work, which imparts commercial impact on the development of non-platinum electrocatalysts for application in AEM alkaline alcohol fuel cells.

1. Introduction

Anion exchange membrane (AEM) alkaline alcohol fuel cells have recently been considered as an alternative power generation source for both mobile and stationary electronics. Anion exchange membrane based direct alkaline alcohol fuel cells (AEM-DAAFCs) have attracted growing interests due to their eco-friendly inexpensive operation with high energy and power density[1,2]. AEM-DAAFCs are promising electrochemical energy convertor that own particular advantages on the possibility of using non-precious metal catalysts[1]. One of the main research areas of AEM-DAAFCs are the development of non-precious metal based oxide catalysts with sufficient activity and prolonged durability. Significant attention has been focused on the synthesis of nanostructured catalyst using earth-abundant elements which is known to act as the alternatives for expensive platinum based catalysts.[1,2] Direct oxidation of fuels on the anode and four electron reduction of molecular oxygen on the cathode in alkaline media are the major process in AEM-DAAFCs. A lot of research efforts have been invested in developing inexpensive and efficient electrocatalysts for direct methanol oxidation and oxygen reduction in alkaline environments.[3-8] AEM-DAAFCs would be beneficial for methanol-oxygen redox system because methanol oxidation reaction (MOR) and oxygen reduction reaction (ORR) occur more easily with faster electrode kinetics in alkaline conditions.[7,8]

Recently, mixed valent transition metal oxides such as Co_3O_4 and $Ni_1Co_2O_4$ are known to act as efficient non-precious catalysts due to their promising activity comparable to platinum based catalysts. They are more stable, less-corrosive and exhibit high electrocatalytic activity at higher pH. Co_3O_4 and $Ni_1Co_2O_4$ with spinel structure are the most widely investigated non-platinum catalysts in ORR and MOR in alkaline media as well as oxygen evolution reaction.[9-15] A bimetallic nickel cobaltite ($Ni_1Co_2O_4$) possesses richer redox chemistry and much better electronic conductivity than nickel and cobalt oxide alone. In general, Ni doping tends to enhance the electrocatalytic efficiency of Co_3O_4 and it has been addressed for $Ni_1Co_2O_4$ in literature.[12-15] On the other hand, shape control of Co-based 1D mixed valent transition metal oxide nanostructures creates new insights in designing the heterogeneous catalyst with unique catalytic properties.[6,16] The creation of 3D hierarchical nanostructures composed of 1D structure would be great significance for AEM-DAAFCs. Therefore, the exploration of the structure, composition and morphology related catalytic activity on these Co_3O_4 and Co-based spinal oxide nanostructures are remains an area of extensive interest.

Despite tremendous efforts, developing electrode catalysts with high conductivity and high catalytic activity are the key requirement of AEM-DAAFCs. Schematic representations of the AEM-DAAFC is shown in Fig. 1, in which methanol is used as fuel and molecular oxygen is used as an oxidant. High performance electrode materials with sufficient activity and durability are anticipated for the commercial development of AEM-DAAFCs with high power and energy densities. One effective way to achieve the advancement of AEM-DAAFCs is to explore the bifunctional catalysts for the MOR and ORR. Many reports have been clearly pointed out the enhanced electrical conductivity and electrocatalytic activity of $Ni_xCo_{3-x}O_4$,[12-15] but its structure, morphology and composition related electrocatalytic activity is not fully understood. The major objective of this work is to understand comprehensively the structure, morphology and composition related electrocatalytic properties of $Ni_xCo_{3-x}O_4$, because development of electrode materials

based on $Ni_xCo_{3-x}O_4$ is highly desirable for the advancement of inexpensive AEM-DAAFCs.

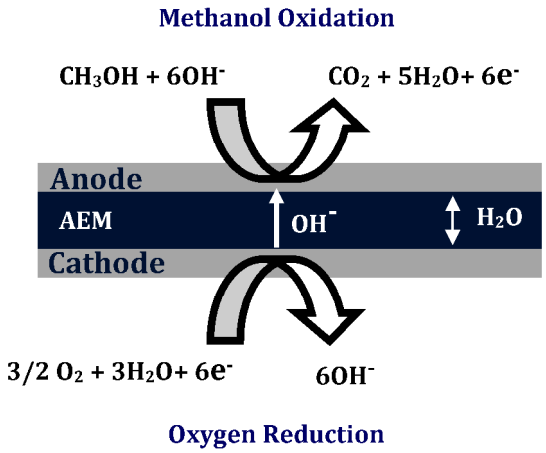

Fig. 1. A schematic diagram and electrode reactions of the AEM-DAAFC.

In this report, series of urchin like spinel Co_3O_4, $Ni_xCo_{3-x}O_4$ and cubic $Co_{0.33}Ni_{0.67}O$ 3D hierarchical nanostructures composed of 1D nanorods were synthesized using simple and reproducible hydrothermal route. The catalytic screening of spinel $Ni_xCo_{3-x}O_4$ along with spinel Co_3O_4 and cubic $Co_{0.33}Ni_{0.67}O$ were successfully explored in this work to explain the observed enhancement in MOR and ORR in alkaline conditions. To the best of our knowledge, the comprehensive synthesis and electrocatalytic evaluation of spinel $Ni_xCo_{3-x}O_4$ 3D hierarchical nanostructures for the MOR and ORR in alkaline media is not explored elsewhere.

2. Experimental

2.1 Materials

Cobalt chloride ($CoCl_2{\cdot}6H_2O$, 99%), Nickel chloride ($NiCl_2{\cdot}6H_2O$, 99.9%), Urea (NH_2CONH_2, 99%) and Nafion perfluorinated ion-exchange resin (eq. wt. 1100) 5 wt.% in mixture of lower aliphatic alcohols and water (45%) were purchased from Sigma-Aldrich. Methanol (99.5%) and ethanol were purchased from Samchun Pure Chemicals Co. Ltd., Korea. Ultra pure water (18 MΩ·cm) was obtained from a μ pure HIQ water purifying system. The glassy carbon electrode (3 mm diameter, geometrical area 0.07 cm^2) purchased from CH Instruments, USA was used for the electrochemical studies.

2.2 Synthesis of Co_3O_4, $Ni_xCo_{3-x}O_4$ and $Co_{0.33}Ni_{0.67}O$ 3D hierarchical nanostructures

The synthesis of Co_3O_4, $Ni_xCo_{3-x}O_4$ and $Co_{0.33}Ni_{0.67}O$ 3D hierarchical nanostructures were carried out *via* a facile hydrothermal method. For the preparation of Co_3O_4 samples, 1 mmol $CoCl_2{\cdot}6H_2O$ and 5 mmol urea (NH_2CONH_2) was dissolved in 75 mL of ultra pure water followed by stirring at room temperature (RT) for 1 h. The obtained pink colored mixture was transferred to Teflon lined stainless steel autoclave (100 mL) and then, the autoclave was kept at 120 °C for 12 h in hot air oven. After 12 h, autoclave was taken out from oven and cooled down to RT. The products were collected by centrifugation, and washed 3 times with water and ethanol, respectively. Then, the product was dried at 80 °C for 6 h in hot air oven and subsequently heated in static air at 300°C for 2h to obtain the final product. The above described protocol was repeated for the synthesis of $Ni_{0.25}Co_{2.75}O_4$, $Ni_{0.50}Co_{2.50}O_4$, $Ni_{0.75}Co_{2.25}O_4$, $Ni_1Co_2O_4$ and $Co_{0.33}Ni_{0.67}O$ samples using the different mole ratio of $NiCl_2{\cdot}6H_2O$ and $CoCl_2{\cdot}6H_2O$ respectively 0.083 : 0.917 mmol, 0.166 : 0.834 mmol, 0.250 : 0.750 mmol, 0.333 : 0.667 mmol and 0.667 : 0.333 mmol.

2.3 Characterizations

Crystallinity of the samples was characterized by an X-ray diffraction (XRD, Rigaku Miniflex II). The morphology and chemical compositions of the Co_3O_4 and Ni/Co bimetallic oxides have been analysed using field emission scanning electron microscopy (FE-SEM, Hitachi S-4800 UHR) with a Bruker energy dispersive X-ray (EDX) system, at an accelerating voltage of 3 kV, and the details of the EDX profile was given in the electronic supplementary information (ESI†). Elemental composition and its chemical and electronic states were determined through X-ray photoelectron spectroscopy (XPS, Multilab ESCA 2000). Transmission electron microscopy (TEM) and high-resolution TEM (HRTEM) images with selected area electron diffraction (SAED) patterns were obtained on a JEM-2100F (JEOL, Japan) at an accelerating voltage of 200 kV. Brunauer-Emmett-Teller (BET) surface area, Barrett-Joyner-Halenda (BJH) cumulative pore area, pore size and pore volume were determined using an ASAP- 2420 accelerated surface area and porosimetry system (Micromeritics, USA). All the electrochemical and rotating disk electrode (RDE) measurements were performed with a BAS100B/W electrochemical workstation (BASi, Indiana) in a three electrode cell arrangement.

2.4 Electrochemical measurements

Linear sweep and cyclic voltammetry experiments were conducted in a three-electrode electrochemical cell using a bare or modified glassy carbon electrode (GCE) as the working electrode, Pt wire as the counter electrode, and Ag/AgCl as the reference electrode. Prior to electrode modification, the surface of GCE was polished to mirror like finish using 0.3μm alumina slurry and then washed few minutes with water and ethanol in an ultra sonicator bath. Before modification, the cleaned GCE was dried using a high-purity nitrogen spray. For the electrode modification, 5 mg of the catalyst and 50 μL Nafion solutions were ultrasonically dispersed in 1 mL of methanol solution and then, the dispersion was ultrasonicated for 30 min to obtain a homogeneous solution of catalyst ink. Then, 5μL of catalyst ink was carefully dropped on the pre-cleaned GCE surface and dried at room temperature to achieve the modified electrode with active catalyst layer. The catalyst loading was constant (~ 0.35 mg cm^{-2}) for all samples. The above described protocol was precisely repeated for the construction of other modified electrodes. All the CV experiments were done at room temperature in 0.1 M KOH solution. Before the electrochemical measurements, the electrodes were cycled at 50 mV s^{-1} between 0 and 600 mV under saturated nitrogen atmosphere until reproducible cyclic voltammograms were obtained. CV curves for MOR were obtained using the various catalyst modified electrodes in the potential region from 0 to 600 mV in 0.1 M KOH with 0.5 M methanol under saturated nitrogen atmosphere. ORR was performed in 0.1 M KOH saturated with oxygen using the various catalyst modified electrodes in the potential region from 0 to - 600 mV. Current densities are given in terms of geometrical area (mA cm^{-2}).

3. Results and Discussions

Crystal structure of the as-synthesized samples was examined by XRD as shown in Fig. 2. XRD patterns are representative for Co_3O_4, $Ni_{0.25}Co_{2.75}O_4$, $Ni_{0.50}Co_{2.50}O_4$, $Ni_{0.75}Co_{2.25}O_4$, $Ni_1Co_2O_4$ and $Co_{0.33}Ni_{0.67}O$, respectively. All the peak patterns except $Co_{0.33}Ni_{0.67}O$ can be obviously indexed as face-

centered cubic spinel structure with a space group of Fd3m (JCPDS Card no. 80-1542).

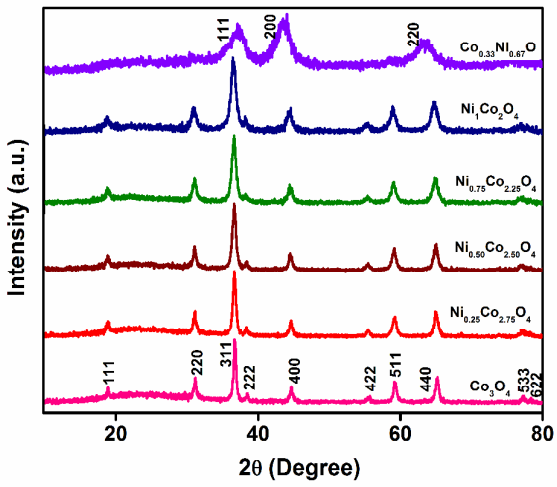

Fig.2. XRD patterns of Co_3O_4, $Ni_xCo_{3-x}O_4$ and $Co_{0.33}Ni_{0.67}O$.

The substitution of Ni for Co does not modify the general aspect of the XRD pattern of Co_3O_4 up to Ni composition of 1 ($Ni_xCo_{3-x}O_4$, $x \leq 1$). However, Ni doping broadens the diffraction line of Co_3O_4 with slight lower shifting of 2θ values, as can be observed from expanded (311) XRD peaks (Fig. S1, ESI†). When the composition of Ni is greater than 1 (i.e. $x = 2$, $Co_{0.33}Ni_{0.67}O$), the characteristics peaks of cubic NiO with a space group of Fm3m was appeared (JCPDS Card no. 04-8350). Thus, the formation of spinel $Ni_xCo_{3-x}O_4$ and cubic $Co_{0.33}Ni_{0.67}O$ has been linked to the compositions of Ni.[18] The average crystallite sizes of samples were calculated using the Scherrer's formula.[17] The crystallite sizes of the $Ni_xCo_{3-x}O_4$ with Ni compositions (x) of 0, 0.25, 0.50, 0.75, and 1 were calculated to be about 19.7, 19.6, 18.9, 16.8 and 16.2 nm, respectively. This indicates that the grain sizes of $Ni_xCo_{3-x}O_4$ were slightly decreased with increasing the Ni composition linearly. In $Co_{0.33}Ni_{0.67}O$, the spinel structure was completely disappeared and leads to pure cubic NiO phase with average crystallite size of 4.5 nm. It can be concluded that by addition of Ni with cubic Co_3O_4, the crystallinity as well as crystalline size are decreased.

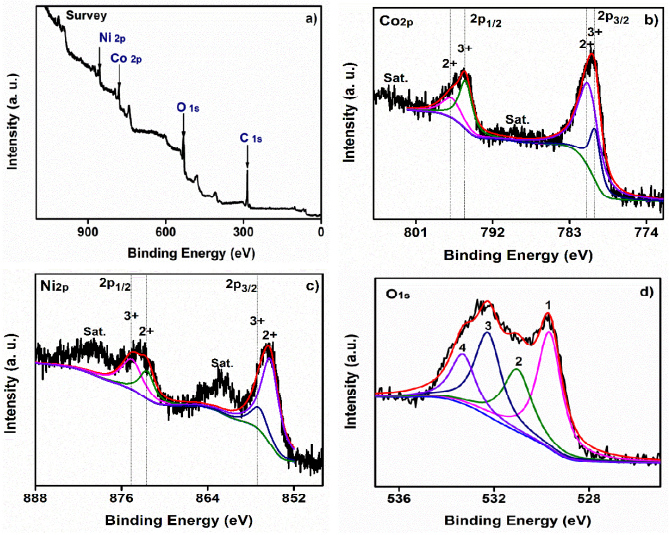

Fig. 3. XPS patterns of proposed $Ni_1Co_2O_4$ catalyst. a) Full scan, b) Co_{2p} core levels, c) Ni_{2p} core levels, d) O_{1s} core levels.

X-ray photoelectron spectroscopy (XPS) was used to determine the chemical and electronic states of Ni and Co in $Ni_xCo_{3-x}O_4$. Fig. 3a-d shows the XPS spectra of the 3D $Ni_1Co_2O_4$ hierarchical nanostructure composed of 1D nanorods after calcinations at 300°C for 2 h. The XPS survey spectrum (Fig. 3a) displays the typical signals of O_{1s}, Co_{2p} and Ni_{2p} core levels. A Gaussian fitting of the Co_{2p} spectrum reveals it consists of two spin-orbit doublets characteristic of Co^{2+} and Co^{3+} and two shakeup (sat.) excitations as shown in Fig. 3b.[15,19] In the same way, Ni_{2p} spectrum (Fig. 3c) of $Ni_1Co_2O_4$ is also consisted of two spin-orbit doublets characteristic of Ni^{2+} and Ni^{3+} and two satellite sub-peaks.[15,19] Fig. 3d shows the high-resolution O_{1s} spectrum of $Ni_1Co_2O_4$ with four oxygen contributions denoted as 1, 2, 3, and 4. The component 1 located at 529.4 eV and the component 2 at 530.2 eV is assigned to metal-oxygen bonds and surface hydroxyl groups, respectively. The component 3 positioned at 532.2 eV is linked with a higher number of defect sites with low oxygen coordination and the component 4 at 533.3 eV is related with a surface bonded water molecules in the samples.[15,19] It can be seen from XPS results that the 3D $Ni_1Co_2O_4$ hierarchical nanostructure composed of 1D nanorods consisting of Co^{2+}, Co^{3+}, Ni^{2+}, and Ni^{3+} species in its structure.[15,19] It was known that Ni ions have a strong tendency to occupy the octahedral sites in spinel lattice.[20] Based on the earlier reports[20] and XPS information, the possible general formula of $Co^{2+}{}_{1-x}Co^{3+}{}_x[Co^{3+}\,Ni^{2+}{}_xNi^{3+}{}_{1-x}]O_4$ ($0 < x \leq 1$) have been proposed for 3D $Ni_xCo_{3-x}O_4$ hierarchical nanostructures. The detailed EDX elemental analysis of $Ni_xCo_{3-x}O_4$ and $Co_{0.33}Ni_{0.67}O$ were given in Fig. S2 (ESI†) for the further support of chemical compositions.

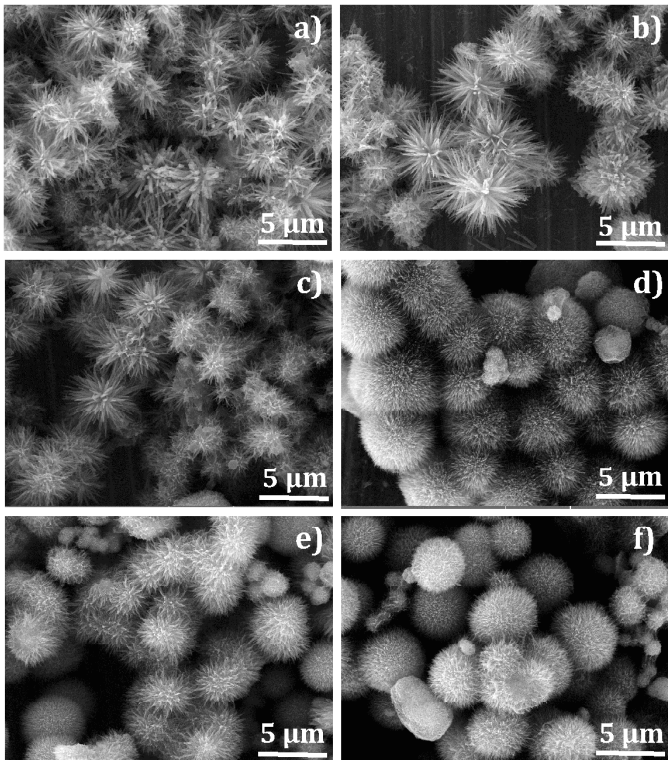

Fig. 4. FE-SEM images of a) Co_3O_4, b) $Ni_{0.25}Co_{2.75}O_4$, c) $Ni_{0.50}Co_{2.50}O_4$, d) $Ni_{0.75}Co_{2.25}O_4$, e) $Ni_1Co_2O_4$ and f) $Co_{0.33}Ni_{0.67}O$.

The FE-SEM images of directly collected Co_3O_4, $Ni_{0.25}Co_{2.75}O_4$, $Ni_{0.50}Co_{2.50}O_4$, $Ni_{0.75}Co_{2.25}O_4$, $Ni_1Co_2O_4$ and $Co_{0.33}Ni_{0.67}O$ samples are respectively shown in Fig. 4a-f. The observed 3D hierarchical nanostructures are uniformly

constructed with 1D nanorods and basically aligned together like a sea-urchin. Average diameters of the sea-urchin like structures are estimated to be ~ 4 µm. It is clear from the Fig. 4d-f that the compositions such as $Ni_{0.75}Co_{2.25}O_4$, $Ni_1Co_2O_4$, and $Co_{0.33}Ni_{0.67}O$ have a fine structure of urchin composed with smooth nanorods which have been assembled into the hierarchical morphology. Structure of the $Ni_1Co_2O_4$ was also investigated by TEM and HRTEM. Fig. 5a shows an assembled structure of 1D nanorods of $Ni_1Co_2O_4$ and Fig. 5b displays porous nature of a nanorod. It can be seen from Fig. 5a and b that the 1D nanorods with diameter of 100-150 nm and length of about 2 µm were constructed by nanoparticles with an average diameter of 20 nm. The HRTEM image (Fig. 5c) shows crystal domains and lattice fringes with spacing of 0.28 nm and 0.24 nm corresponding to the (220) and (311) lattice planes of $Ni_1Co_2O_4$, respectively.[21] The ring patterns of SAED shown in Fig. 5d further support the polycrystalline nature of $Ni_1Co_2O_4$ nanorods. The textural properties of $Ni_xCo_{3-x}O_4$ and $Co_{0.33}Ni_{0.67}O$ hierarchical nanostructures were obtained through N_2 adsorption-desorption isotherm and the details of data profiles are given in Fig. S3 (ESI†). It can be seen from Table S1(ESI†) that the BET surface area, cumulative surface area of pores and total pore volume of spinel $Ni_xCo_{3-x}O_4$ increased with increasing the value of x up to 1. It is important to note that the undoped Co_3O_4 exhibited relatively wide range of mesoporous distribution (10-50 nm) which has been reduced to 2-10 nm up on increasing the Ni content (x = 1, $Ni_1Co_2O_4$). Moreover, the pore diameter also reduced from 23 nm to 11 nm when x is increased from 0.25 to 1 in $Ni_xCo_{3-x}O_4$. However, $Co_{0.33}Ni_{0.67}O$ (x = 2) demonstrated the broad range of pore size distribution (2-100 nm) with decreased BET surface area (120 m^2g^{-1}) and BJH pore area (153 m^2g^{-1}) than $Ni_1Co_2O_4$ (Table S1, ESI†). This could be due to the fact that the spinel structure of $Ni_xCo_{3-x}O_4$ has been totally disappeared by cubic NiO when the mole fraction of Ni is greater than 1 (i.e. x = 2, $Co_{0.33}Ni_{0.67}O$). Surface area and pore size analysis clearly indicates that the $Ni_1Co_2O_4$ catalyst exhibited a typical mesoporous structure with narrow pore size distribution (2-10 nm) and it has high specific surface area (123 m^2g^{-1}) with increased cumulative surface area of pores (156 m^2g^{-1}) than the other catalysts. The obtained textural features of $Ni_1Co_2O_4$ are significantly greater than those of the earlier reports.[3,22,23]

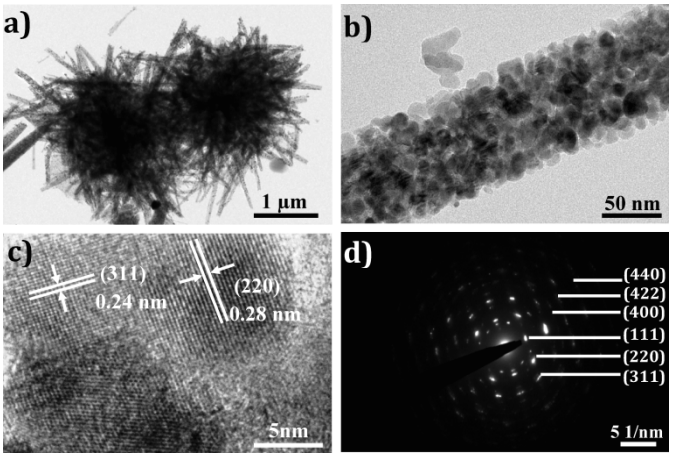

Fig. 5. a) TEM image at 1µm scale bar b) TEM image at 50 nm scale bar c) HRTEM image and d) SAED pattern of the proposed $Ni_1Co_2O_4$ nanostructure.

It can be anticipated that the enhanced textural features of $Ni_1Co_2O_4$ significantly influence the efficient transport of fuels and oxidant to the catalyst active site than the other compositions of nickel cobaltite hierarchical nanostructures. Therefore, the obtained sea-urchin like hierarchical structure with mesoporosity would be more beneficial for MOR and ORR activity and could be useful to AEM-DAAFC electrodes. The CV curves measured in 0.1 M KOH at a scan rate of 50 mV S^{-1} for the Co_3O_4, $Ni_xCo_{3-x}O_4$ and $Co_{0.33}Ni_{0.67}O$ modified electrodes are presented in Fig. 6. As can be seen in Fig. 6, Co_3O_4 modified electrode exhibits the anodic response (initiated at 490 mV) with rapidly increased peak current during the positive scanning from 0 to 600 mV, corresponding to the oxidation of the Co^{3+} species. Consecutively, the cathodic peak at around 540 mV is associated to the reduction of the Co^{4+} to Co^{3+} species on the surface of the Co_3O_4 catalyst. These electrochemical responses are the characteristics of surface confined redox couples of Co_3O_4 which can be described as CoOOH (Co^{3+}) / CoO_2 (Co^{4+})**.** Besides, the CV curves for the $Ni_xCo_{3-x}O_4$ modified electrodes shows a pair of redox couples (CoOOH/CoO_2[8] and NiOOH/NiO_2[24]) with the broad anodic peak which is shifted towards the negative direction (anodic peak potential, Epa ~ 330 mV for $Ni_{0.25}Co_{2.75}O_4$, Epa ~ 315 mV for $Ni_{0.50}Co_{2.50}O_4$ and Epa ~ 300 mV for $Ni_{0.75}Co_{2.25}O_4$ and $Ni_1Co_2O_4$). This potential shift towards more negative (less positive) direction was contributed from Ni^{3+} to Ni^{4+} oxidation along with Co^{3+} to Co^{4+} oxidation on the surface of the $Ni_xCo_{3-x}O_4$ catalyst.[25]

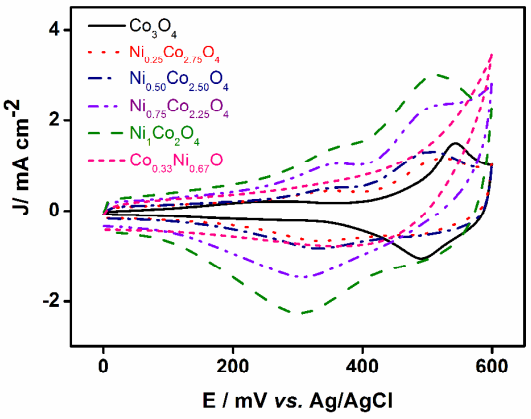

Fig. 6. CV curves measured in 0.1 M KOH at a scan rate of 50 mV S^{-1}.

Upon Ni doping, the peak current densities are gradually increased from 0.66 mA cm^{-2} to 2.25 mA cm^{-2} with increasing the mole fraction (x) of Ni from 0.25 to 1 in $Ni_xCo_{3-x}O_4$. More significantly, the peak current density of $Ni_1Co_2O_4$ electrode (2.25 mA cm^{-2}) was increased twice than the Co_3O_4 electrode (1.05 mA cm^{-2}). Furthermore, the dramatic reductions in anodic peak current density were resulted for $Co_{0.33}Ni_{0.67}O$ electrode (Fig. 6). This is due to the disappearance of spinel structure and the absence of electrochemically active redox couples (Co^{3+}/Co^{4+} and Ni^{3+}/Ni^{4+}). Fig. 7 displays the CV curves for the ORR and MOR characteristics of bare GCE and Co_3O_4, $Ni_xCo_{3-x}O_4$ and $Co_{0.33}Ni_{0.67}O$ hierarchical nanostructures modified GCEs. The linear sweep voltammetry (LSV) curves for the ORR and MOR are shown in Fig. S4 (ESI†) for comparison. It is interesting to note that the ORR activity of Co_3O_4, $Ni_xCo_{3-x}O_4$ and $Co_{0.33}Ni_{0.67}O$ catalysts are strictly repeated and consistent with the electrochemical characteristics observed in Fig. 6. Catalytic activities for the ORR in 0.1 M KOH solution saturated with pure oxygen are shown in Fig. 7a. It was found that $Ni_1Co_2O_4$ catalyst contributes markedly higher ORR activity among

the six catalyst modified electrodes. The MOR activity of Co_3O_4, $Ni_xCo_{3-x}O_4$ and $Co_{0.33}Ni_{0.67}O$ catalysts are shown in Fig. 7b. The value of the MOR current density for the six catalysts, is in the sequence of $Ni_1Co_2O_4$ > $Ni_{0.75}Co_{2.25}O_4$> $Ni_{0.50}Co_{2.50}O_4$ > $Co_{0.33}Ni_{0.67}O$ > $Ni_{0.25}Co_{2.75}O_4$ > Co_3O_4 which is in close resemblance with ORR activity. The plots of Ni mole fraction *versus* onset potential and current density for ORR are shown in Fig. 8a, which has been used to explore the relationship between the catalysts ORR activity and Ni compositions. Current density measurements and onset potential calculations are given in Fig. S5 (ESI†).

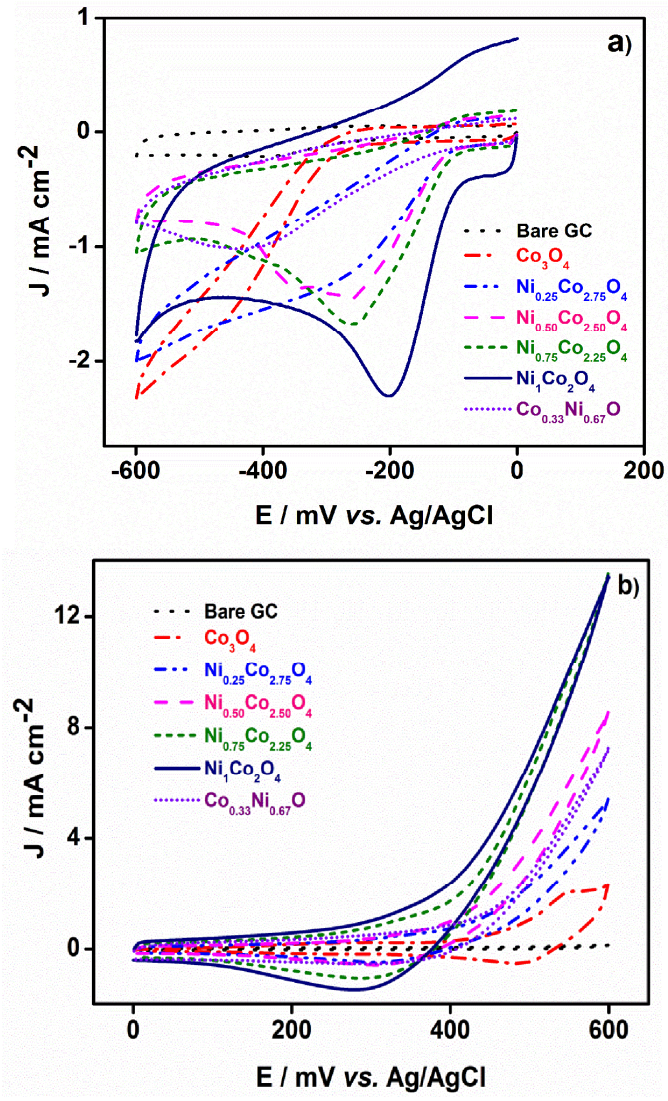

Fig.7. CV curves of a) oxygen reduction reaction (ORR) and b) methanol oxidation reaction (MOR).

Fig. 8a makes visible that Co_3O_4 electrode has better current density (2.33 mA cm^{-2}) nearly close to $Ni_1Co_2O_4$ electrode, but the ORR diffusion region was shifted to more negative onset potential (-285 mV). As can be observed in Fig. 8a, Ni doping initially step-downs the current density and increased to 2.32 mA cm^{-2} for $Ni_1Co_2O_4$ electrode. At the same time, Ni doping shifts the onset potential towards less negative side from -285 mV to -96 mV respectively for Co_3O_4 to $Ni_1Co_2O_4$ electrodes. Obviously, the proposed $Ni_1Co_2O_4$ shows the enhanced ORR activity at less negative onset potential (-96 mV *vs.* Ag/AgCl) with high current density (2.32 mA cm^{-2}) than the other compositions of $Ni_xCo_{3-x}O_4$ and $Co_{0.33}Ni_{0.67}O$ electrodes.

Rotating-disk voltammograms were recorded on hierarchical nanostructures-modified electrodes in O_2-saturated 0.1 M KOH solution at four different (500, 1000, 1500 and 2000 ± 5 rpm) rotation rates to construct a Koutecky-Levich (K–L) plot for ORR. The electron transfer numbers were calculated using the slope of the K-L curve (Fig. S6 & S7, ESI†). Fig. 8b presents the plot of Ni mole fraction *versus* electron transfer number (n). The n value of the $Ni_1Co_2O_4$ was calculated to be 4.18 at -500 mV *vs* Ag/AgCl, higher than those for Co_3O_4 (2.71), $Ni_{0.25}Co_{2.75}O_4$ (1.93), $Ni_{0.50}Co_{2.50}O_4$ (2.16), $Ni_{0.75}Co_{2.25}O_4$ (2.55) and $Co_{0.33}Ni_{0.67}O$ (2.25). This suggests that $Ni_1Co_2O_4$ follow an efficient four electron pathway while all other catalysts nearly follow two electron pathways. Fig. 8a and b make visible that current density and electron transfer number are interrelated, indicates that the proposed $Ni_1Co_2O_4$ system more efficiently reduces the oxygen molecule and significantly contributes higher current density at low onset potential.

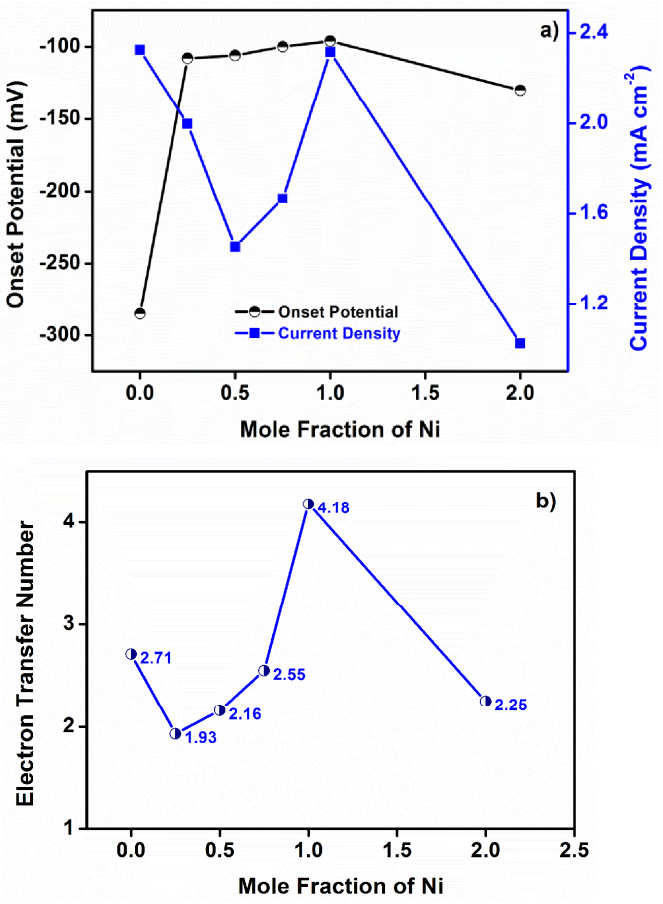

Fig.8. Plots of Ni mole fraction *versus* onset potential (a), current density (a) and electron transfer numbers (b) for ORR.

This is inferred that the less negative shifting of onset potential for four electron oxygen reduction requires more active sites (Co^{3+} and Ni^{3+}) that may be obtained by the doping fraction of Ni (x) around 1. The improved textural features of $Ni_1Co_2O_4$ (Table S1, ESI†) could provides sufficiently exposed Ni^{3+} and Co^{3+} species on the octahedral site which can produce more surface

electronic states by the Jahn-Teller effect[8] in alkaline media. These surface electronic states with high electron density contribute the better ORR activity of $Ni_1Co_2O_4$. The relative catalytic behaviours of Co_3O_4, $Ni_xCo_{3-x}O_4$ and $Co_{0.33}Ni_{0.67}O$ catalysts for the MOR in 0.1 M KOH solutions with 0.5 M CH_3OH is shown in Fig. 9a. The profile data for MOR are given in Fig. S8 (ESI†). Upon Ni doping, the onset potential was shifted from more positive (499 mV) to less positive (300 mV) when the mole fraction of nickel changed from 0 to 1. It can be seen from Fig. 9a that the Co_3O_4 catalyst shows the lower current density (2.30 mA cm^{-2}) at more positive onset potential (499 mV), while the $Ni_1Co_2O_4$ catalyst show higher current density (13.49 mA cm^{-2}) at less positive onset potential (300 mV) for the MOR. Also, $Ni_1Co_2O_4$ was identified as an efficient catalyst for the MOR among the six catalysts explored in this study.

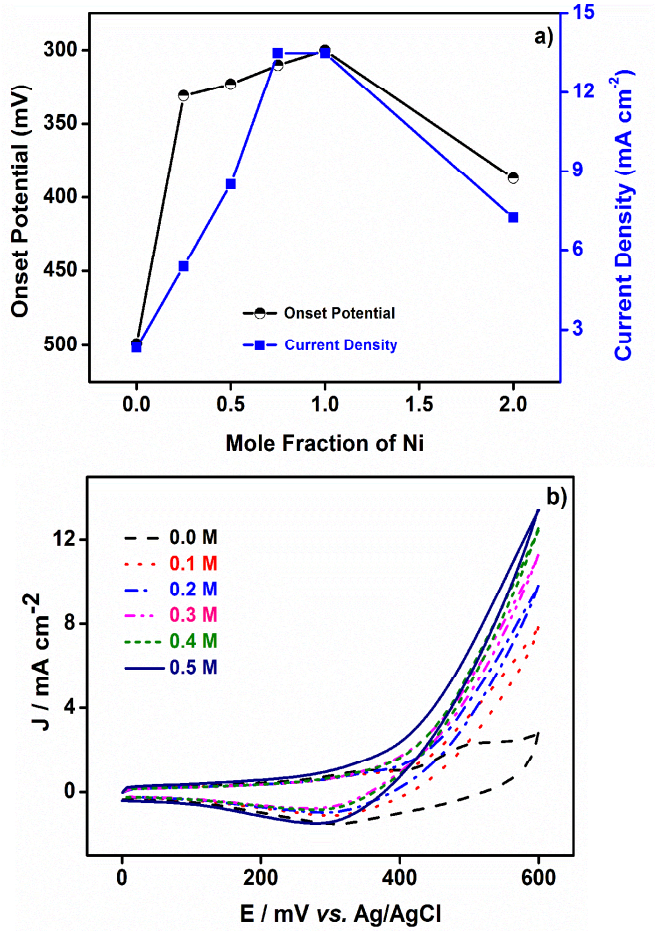

Fig.9. a) Plot of Ni mole fractions *versus* onset potential and current density and b) CV curves measured in 0.1 M KOH solutions with different concentrations of CH_3OH at 50 mV s^{-1}.

As expected, the improved surface features of $Ni_1Co_2O_4$ (Table S1, ESI†) hierarchical nanostructure provides highly exposed active sites (Ni^{3+} and Co^{3+}) for methanol oxidation, which imparts higher current density with reduced over potential. It is important to note that the sub-micrometer particle (crystallite) sizes of $Ni_xCo_{3-x}O_4$ are decreased with increasing the nickel content. Crystal size reduction enhances the electrocatalytic activity of $Ni_xCo_{3-x}O_4$ by providing more surface catalytic sites which make the system ($Ni_1Co_2O_4$) more active. Further, the large accessible surface area (123 m^2g^{-1}) with an exposed pore area of 156 m^2g^{-1} is more significant for the observed enhancement in proposed $Ni_1Co_2O_4$. Thus, the $Ni_1Co_2O_4$ catalyst hands on the enhancement of MOR and ORR kinetics at diffusion controlled region than the other catalysts. It can be concluded that the improved textural features of $Ni_1Co_2O_4$ (Table S1, ESI†) significantly contributes enhanced ORR and MOR activity. Therefore, $Ni_1Co_2O_4$ electrode was selected as potential anode and cathode for both the MOR and ORR activity. It is necessary to explore the influence of CH_3OH concentrations on the catalytic behaviour of proposed $Ni_1Co_2O_4$ hierarchical nanostructure, in order to understand the sensitivity of the electrode.

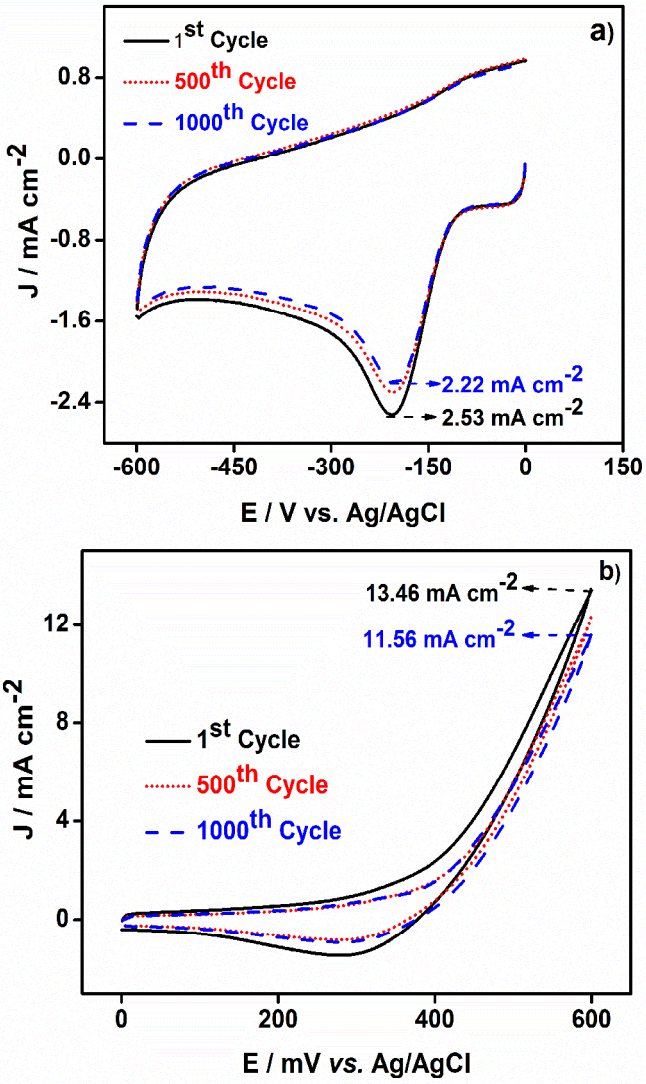

Fig.10. CV curves measured in 0.1 M KOH solutions with a) saturated oxygen and b) 0.5 M CH_3OH obtained after 1st cycle and after 1000 cycles at 50 mV s^{-1}.

Fig. 9b displays the concentrations dependent electrocatalytic ability of $Ni_1Co_2O_4$ catalyst. In absence of CH_3OH, the proposed $Ni_1Co_2O_4$ electrode shows one pair of broad redox peaks which has been originated from the charge transfer processes of solid state redox couples (Co^{3+} Ni^{3+}/$Co^{4+}Ni^{4+}$).[8,24] As can be seen in Fig. 9b, the limiting current density increased almost linearly with increasing CH_3OH concentrations. The peak current densities are found to be 7.82, 9.80, 11.25, 12.49 and 13.37 mA cm^{-2} for 0.1, 0.2, 0.3, 0.4 and 0.5 M concentrations of CH_3OH, respectively. The onset potential slightly shifted towards positive side when increasing the

CH_3OH concentrations from 0.1 M to 0.5 M. The reliability of $Ni_1Co_2O_4$ hierarchical nanostructure modified electrode towards ORR and MOR was also examined by CV cycling test. Fig. 10a depicts the CV curves of proposed $Ni_1Co_2O_4$ electrode in 0.1 M KOH solutions saturated with pure oxygen. It can be clearly seen that the CV curves are quite stable and the current density at -200 mV (vs. Ag/AgCl) exhibits 87 % retention (decayed from 2.53 to 2.22 mA cm^{-2}) after 1000 cycles. The CV curves of proposed $Ni_1Co_2O_4$ electrode in mixture of 0.1 M KOH and 0.5 M CH_3OH solutions saturated with nitrogen are presented in Fig. 10b. As shown in Fig. 10b, the performance of proposed $Ni_1Co_2O_4$ electrode for the MOR has slightly decayed (from 13.46 to 11.56 mA cm^{-2}) and the current density at 600 mV (vs. Ag/AgCl) exhibits 85 % retention after 1000 CV cycles. Thus, the proposed $Ni_1Co_2O_4$ electrode shows good sensitivity and better stability for the ORR and MOR activity. In summary, the fraction of Ni in $Ni_xCo_{3-x}O_4$ significantly alters the onset potential and current density towards positive direction by providing two kinds of active sites (surface exposed Ni^{3+} and Co^{3+} species) for both ORR and MOR. These results suggest that the 3D $Ni_1Co_2O_4$ hierarchical nanostructure composed with 1D nanorods are promising non-precious electrocatalysts for AEM-DAAFC. The developed $Ni_1Co_2O_4$ catalysts may be transferred to fabrication of inexpensive AEM-DAAFC electrodes in future.

4. Conclusions

In conclusion, we have developed a comprehensive approach for synthesis of series of nickel cobaltite 3D hierarchical nanostructures by a facile hydrothermal route. In this series, high surface area (123 m^2g^{-1}) mesoporous 3D $Ni_1Co_2O_4$ hierarchical nanostructure with an exposed pore area of 156 m^2g^{-1} have been synthesized and optimised for efficient MOR and ORR activity. Changing the mole fraction of Ni in $Ni_xCo_{3-x}O_4$ affects the exposed active sites which influences the catalytic properties of the 3D hierarchical nanostructures. Although Co_3O_4 or $Co_{0.33}Ni_{0.67}O$ alone has moderate catalytic activity, $Ni_1Co_2O_4$ exhibit high ORR and MOR activities with reliable stability and durability. In addition, $Ni_1Co_2O_4$ electrode shows significantly improved onset potential and current density compared to the earlier reports. This is a first time effort for the comparative electrocatalytic evaluation of ternary nickel cobaltite 3D hierarchical nanostructures. This opens up an inexpensive approach to develop highly promising and non-precious, bi-functional catalysts for AEM-DAAFCs.

Acknowledgements

This work was financially supported by Basic Science Research Program (2012R1A1A2043731) through the National Research Foundation, Korea.

Notes and references

Author information

Department of Chemistry and GETRC, Kongju National University, 182, Shinkwondong, Kongju, 314-701, Chungnam-do, Republic of Korea

*Corresponding Author
E-mail: jkim@kongju.ac.kr, Fax: +82-41-850-8613;
Tel: +82-41-850-8496.

Supporting Information

Electronic Supplementary Information (ESI†) available: EDX profiles of $Ni_xCo_{3-x}O_4$ and $Co_{0.33}Ni_{0.67}O$ 3D hierarchical nanostructures, BET surface area and pore size distribution data, LSV data for all the catalysts and individual CV data with onset potential and current density measurement details. See DOI: xxx/xxx/

1. E. H. Yu, X. Wang, U. Krewer, L. Lid and K. Scott, *Energy Environ. Sci.,* 2012, **5,** 5668.
2. Q. He, Q. Li, S. Khene, X. Ren, F. E. Lopez-Suarez, D. Lozano-Castello, A. Bueno-Lopez and G. Wu, *J. Phys. Chem. C,* 2013, **117,** 8697.
3. L. Qian, L. Gu, L.Yang, H. Yuanb and D. Xiao, *Nanoscale,* 2013, **5,** 7388.
4. Y. Liang, Y. Li, H. Wang, J. Zhou, J. Wang, T. Regier and H. Dai1, *Nature Materials,* 2011, **10,** 780.
5. S. Jiang, C. Zhu and S. Dong, *J. Mater. Chem. A,* 2013, **1,** 3593.
6. M. Hamdani, R.N. Singh and P. Chartier, *Int. J. Electrochem. Sci.,* 2010, **5,** 556.
7. A. Morgan, R. Kavanagh, W. Lin, C. Hardacre and P. Hu, *Phys.Chem. Chem. Phys.,* 2013,**15,** 20170.
8. J. Xu, P. Gaob and T. S. Zhao, *Energy Environ. Sci.,* 2012, **5,** 5333.
9. B.H. R. Suryanto, X. Lu and C. Zhao, *J. Mater. Chem. A,* 2013, **1,** 12726.
10. D. Wang, X. Chen, D. G. Evans and W. Yang, *Nanoscale,* 2013, **5,** 5312.
11. Y. J. Sa, K. Kwon, J. Y. Cheon, F. Kleitzc and S. H. Joo, *J. Mater. Chem. A,* 2013, **1,** 9992.
12. C. Jin, F. Lu, X. Cao, Z. Yang and R. Yang, *J. Mater. Chem. A,* 2013, **1,** 12170.
13. N. Garg, M. Basu, K. Upadhyaya, S. M. Shivaprasad and A. K. Ganguli, *RSC Adv.,* 2013, **3,** 24328.
14. Y. Li, P. Hasin, and Y. Wu, *Adv. Mater.,* 2010, **22,** 1926.
15. R. Ding, L. Qi, M. Jiac and H. Wang, *Catal. Sci. Technol.,* 2013, **3,** 3207.
16. Q. Zhang, H.Y. Wang, X. Jia, B. Liu and Y. Yang, *Nanoscale,* 2013, **5,** 7175.
17. P. Ramasamy, S. I. Mamum, J. Jang and J. Kim, *CrystEngComm,* 2013, **15,** 2061.
18. Y. E. Roginskaya, O. V. Morozova, E. N. Lubnin, Y. E. Ulitina, G. V. Lopukhova and S. Trasatti, *Langmuir,* 1997, **13,** 4621.
19. R. Zou, K. Xu, T.Wang, G. He, Q. Liu, X. Liu, Z. Zhang and J. Hu, *J. Mater. Chem. A,* 2013, **1,** 8560.
20. J. G. Kim, D. L. Pugmire, D. Battaglia and M. A. Langell, *Appl. Surf. Sci.,* 2000, **165,** 70.
21. H. L. Wang, Q. M. Gao and L. Jiang, *Small,* 2011, **7,** 2454.
22. D. U. Lee, B. J. Kim and Z. Chen, *J. Mater. Chem. A,* 2013, **1,** 4754.
23. Q. Wang, B. Liu, X. Wang, S. Ran, L. Wang, D. Chen and G. Shen, *J. Mater. Chem.,* 2012, **22,** 21647.
24. M. E. G. Lyons and M. P. Brandon, *Int. J. Electrochem. Sci.,* 2008, **3,** 1386.
25. P. Rasiyah, A. C. C. Tseung and D. B. Hibbert, *J. Electrochem. Soc.,* 1982, **129,** 1724.